Title

Transforming understanding of paleomagnetic recording: Insights from experimental observations of laboratory aged thermal remanences

Authors

Tauxe, Lisa
Santos, Christeanne
Zhao, Xiang
et al.

Publication Date

2020-03-23

DOI

10.5194/egusphere-egu2020-1960

Peer reviewed

Geochemistry, Geophysics, Geosystems

RESEARCH ARTICLE
10.1029/2018GC007946

Investigating the Accuracy, Precision, and Cooling Rate Dependence of Laboratory-Acquired Thermal Remanences During Paleointensity Experiments

C. N. Santos[1] and L. Tauxe[1]

[1]Scripps Institution of Oceanography, La Jolla, CA, USA

Key Points:
- Paleointensity experiments confirm that ideally behaved specimens can give highly accurate and precise paleofield estimates
- Experiments that have curved NRM/TRM plots have much more scattered (although unbiased) estimates
- Experiments from a range of domain states exhibited significant dependence of thermal remanence on cooling rate

Correspondence to:
L. Tauxe,
ltauxe@ucsd.edu

Citation:
Santos, C. N., & Tauxe, L. (2019). Investigating the accuracy, precision, and cooling rate dependence of laboratory-acquired thermal remanences during paleointensity experiments. *Geochemistry, Geophysics, Geosystems*, *20*. https://doi.org/10.1029/2018GC007946

Received 6 SEP 2018
Accepted 21 DEC 2018
Accepted article online 27 DEC 2018

Abstract We examine the behavior of natural basaltic and trachytic samples during paleointensity experiments on both the original and laboratory-acquired thermal remanences and characterize the samples using proxies for domain state including curvature (k) and the bulk domain stability parameters of Paterson (2011, https://doi.org/10.1029/2011JB008369) and Paterson et al. (2017, https://doi.org/10.1073/pnas.1714047114), respectively. A curvature value of 0.164 (suggested by Paterson, 2011, https://doi.org/10.1029/2011JB008369) as a critical threshold that separates single-domain-like remanences from multidomain-like remanances on the original paleointensity data was used to separate samples into "straight" (single-domain-like) and "curved" (multidomain-like) groups. Specimens from the two sample sets were given a "fresh" thermal remanent magnetization in a 70 μT field and subjected to an infield-zerofield, zerofield-infield (IZZI)-type (Yu et al., 2004, https://doi.org/10.1029/2003GC000630) paleointensity experiment. The straight sample set recovered the laboratory field with high precision while the curved set had much more scattered results (70.5 $\pm$ 1.5 and 71.9 $\pm$ 5.2 μT, respectively). The average intensity of both sets for straight and curved was quite close to the laboratory field of 70 μT, however, suggesting that if experiments contain a sufficient number of specimens, there does not seem to be a large bias in the field estimate. We found that the dependence of the laboratory thermal remanent magnetization on cooling rate was significant in most samples and did not depend on domain states inferred from proxies based on hysteresis measurements and should be estimated for all samples whose cooling rates differ from that used in the laboratory.

Plain Language Summary The strength of the magnetic field is one of the fundamental properties of the Earth, and its behavior over time has implications in disparate fields from geodynamics to archeology. Of all the forms of remanent magnetization found in nature, thermal remanent magnetization has the strongest theoretical basis and natural and archeological materials have been used for decades to estimate ancient field strengths. In this paper, we examine the behavior of a variety of rocks typically used for such experiments to investigate their capacity to retain a record of the field. Our results confirm that while ideally behaved specimens (those that give linear plots relating natural and laboratory partial thermal remanences) can give highly accurate and precise paleofield estimates, those that have curved plots have much more scattered (although unbiased) estimates.

1. Introduction

The strength of the magnetic field is one of the fundamental properties of the Earth, and its behavior over time has implications in disparate fields from geodynamics (e.g., Biggin et al., 2012) to archeology (e.g., Ben-Yosef et al., 2010). Of all the forms of remanent magnetization found in nature, thermal remanent magnetization (TRM) has the strongest theoretical basis thanks to the work of Néel (1949) and Thellier and Thellier (1959), supported by experimental evidence by, for example, Wernsdorfer et al. (1997). TRM is related to the ambient magnetic field applied during cooling by a hyperbolic tangent function, which is quasi-linear for low fields like the Earth's and can be reproduced in the laboratory, making absolute paleointensity estimates possible. Yet the optimization of techniques for paleointensity determination has been a longstanding debate in the paleomagnetic community (e.g., Dunlop, 2011). The complexities and

ambiguities both in the field and in the laboratory have fostered a multiplicity of approaches to the problem of intensity estimation.

As an example of the complexity of TRM, it has long been suspected that cooling rate may have a strong effect, resulting in either an overestimate or an underestimate of the ancient magnetic field (e.g., Thellier, 1938). Despite decades of research, the magnitude and mechanisms controlling the cooling rate dependence of TRM are still subject to debate with some suggesting that remanence dominated by single-domain (SD) particles show a strong cooling rate dependence, while so-called "pseudo-single-domain" (PSD) and multidomain (MD) remanences shown no or even a negative cooling rate dependence, respectively (e.g., Biggin et al., 2013; Ferk et al., 2014).

In this paper we examine the theoretical and experimental constraints on cooling rate from previously published literature in section 2. In section 3 we describe rock magnetic and paleointensity experiments on a sample set selected based on the behavior in published paleointensity experimental data, which allow us to separate the samples into "SD like," with nearly straight Arai plots (Nagata et al., 1963) of the original paleointensity data and "non-SD like" with significantly curved Arai plots using the curvature criterion of Paterson (2011). In section 4 we present the results of our experiments on fresh laboratory-acquired TRMs, and in section 5 we discuss implications for the accuracy and precision of paleointensity estimates of the SD-like specimens versus those with in the "curved" category and compare cooling rate dependence of the remanence with various domain state proxies. Our conclusions are summarized in section 6.

2. Background for Cooling Rate Dependence

Starting with Néel (1949), many authors have predicted that the thermally blocked remanent magnetization acquired by a sample will depend on the rate at which it cools. This phenomenon results from the dependence of blocking temperature on cooling rate. Blocking temperature (T_b) is the temperature at which a population of magnetic grains goes abruptly from maintaining equilibrium with an external field to being "blocked" and unable to maintain equilibrium during cooling at a given rate. T_b depends on relaxation time, τ, which is the time (in seconds) required for the magnetization of a given grain size (and shape) population to decay to $1/e$ of its original magnetization when placed in zero field (see, e.g., Tauxe et al., 2010, for a review); therefore, τ is strongly dependent on temperature, so T_b is inherently rate dependent. Because the relaxation time of a given grain increases with decreasing temperature, Néel theory for SD magnetizations predicts that the more slowly a sample cools, the longer equilibrium magnetization can be maintained and the stronger the net magnetization will be.

The problem with this simple theory from a practical standpoint of, say, correcting for cooling rate dependence from first principles is that such a correction requires integration of nonlinear differential equations that are based on a number of poorly constrained assumptions including, for example, that the grains are uniaxial, noninteracting, and SD, assumptions rarely met in natural materials. If magnetic grains are SD, but not uniaxial, which may be much more common in nature than previously thought (e.g., Mitra et al., 2011), the energy landscape may be more complex, although the net effect of this appears to be minimal (e.g., Newell, 2017). What is clear, however, is that different approaches to the cooling rate problem have led to different predictions regarding the dependence of magnetization and cooling rate as outlined in the following.

2.1. SD Magnetizations

Drawing on the theory of Néel (1949), Stacey (1963) predicted a dependence of blocking temperature on the rate at which samples cool through their blocking temperatures whereby noninteracting SD grains would have stronger TRMs when cooled more slowly. York, (1978a, 1978b) expanded on the ideas of Stacey (1963) and developed a function for blocking temperature dependent on cooling rate. York defined blocking temperature by imagining a time t and temperature T_i at which the field is switched off while the sample continues to cool to ambient temperature. If the magnetization has decayed less than 5%, then T_b is estimated by T_i. If the sample cools slowly, the magnetization can maintain equilibrium with the applied field to lower temperatures. Because magnetization is a strong (inverse) function of temperature near the Curie temperature, the net magnetization acquired by slow cooling will be larger than by fast cooling.

Halgedahl et al. (1980) analytically and numerically determined a relationship between cooling rate and the ability of SD magnetite to acquire a TRM. She used the definition for blocking temperature of Néel (1949) whereby at T_b, the relaxation time τ is equivalent to the cooling time interval Δt during which τ changes by

a factor of e. From this it follows that at the blocking temperature T_b,

$$\dot{T}_b \frac{\delta\tau}{\delta T} \simeq \text{const},$$

where $\dot{T}_b$ is the rate of change of T_b and $\frac{\delta\tau}{\delta T}$ is the change of τ with temperature. By making the (Néel) assumption of noninteracting uniaxial particles, she derived an analytical expression relating the laboratory magnetization M_L acquired at a cooling rate ($\dot{T}_{b,L}$ to the magnetization M acquired during a natural cooling rate ($\dot{T}_b$) as

$$\frac{M}{M_L} \simeq 1 + \ln\left(\frac{\dot{T}_b}{\dot{T}_{b,L}}\right)\left(\frac{kT}{2E}\right),$$

where E is the energy barrier between the two easy axes at temperature T and k is Boltzman's constant. Using the Néel relationship for τ to be $\frac{1}{C}\exp\frac{E}{kT}$ and assuming a value for C, the frequency factor, of 10^{-9}/s and a laboratory value for τ to be 10^2 s, Halgedahl et al. (1980) estimated E/kT to be ≃25. So for 1 order of magnitude difference in cooling rate, M is some 1.05 times M_L. She checked this simple analytical approximation with a more sophisticated numerical approach and found that the analytical approximation performed surprisingly well. The Halgedahl equation therefore predicts a ~5% over estimation of paleointensity for each order of magnitude decrease in cooling rate in nature relative to that used in the laboratory experiment and has been used by, for example, Selkin et al. (2000) to correct intrusive Archean samples for the effect of slow cooling.

Dodson and McClelland-Brown (1980) started from the same Néel assumptions and derived a relationship between magnetization and changes in blocking temperature that result from changes in cooling rate:

$$\frac{\Delta n_b}{n_b} = -\frac{\Delta T_b}{T_b}\left(1 - \frac{T}{M_s}\frac{\delta M_s}{\delta T}\right),$$

where n_b is the magnetization blocked at T_b, Δn_B is that blocked at ΔT_b, M_s is saturation magnetization, and $\frac{\delta M_s}{\delta T}$ is the change in saturation with temperature. While not as straightforward as the Halgedahl expression, they calculated that $\frac{\Delta n_b}{n_b}$ would be about 7% larger for each order of magnitude difference in cooling rate.

In the same year, Fox and Aitken (1980) compiled results from unpublished data in PhD theses of N. J Dunn and J. M. W. Fox and new experiments comparing slowly cooled remanences (cooling times of 2, 2.5, and 16 hr) with those acquired over rapid (cooling times of 3 or 5 min). All of their experiments resulted in higher magnetizations in the slower cooled cases. They reported overestimates of 2–9% for a 2-hr cooling. Assuming that the ratios of cooling times are the same as the ratios between cooling rates at the time of blocking, we can compare their results with the predictions of Halgedahl et al. (1980) and Dodson and McClelland-Brown (1980). The sense of the cooling rate dependence is the same (slower cooling leads to higher magnetization), and the magnitudes are similar as well (6% and 10% predicted by Halgedahl et al., 1980, and Dodson & McClelland-Brown, 1980, respectively) 5% for a 2.5-hr cooling (compared to the predicted ~8% and 10%) and 7–14% for the 16-hr cooling (compared to predictions of 13% and 16%).

McClelland-Brown (1984) repeated the experiments of Fox and Aitken (1980) on synthetic magnetites and titanomagnetites of various sizes and concentrations using cooling times of 2.5 hr and 3 min for the slow and fast-cooling experiments, respectively. For the noninteracting SD (100- to 180-μm acicular magnetite) she found a 15% overestimate (compared to predictions of 9% and 12% from Halgedahl et al., 1980, and Dodson & McClelland-Brown, 1980, respectively). For the interacting SD experiment, she found that the fast-cooled experiment was about 5% greater than the slow-cooled one, an opposite effect than that predicted by Néel theory.

Ferk et al. (2010), see also Ferk et al. (2014), analyzed the cooling rate effect for synthetic volcanic glass under a range of laboratory cooling rates (from 0.1 to 15 K/min) and found that the slowest-cooled experiments had an 18% larger paleointensity estimate than the laboratory field.

Yu (2011) analyzed synthetic and natural SD samples in cooling rates of 40 and 3 K/min for fast and slow cooling. He found overestimates of the slow cooling relative to the fast cooling ranging from 3% to 20%.

Berndt et al. (2017) reprised the theoretical development of Néel (1949), York, (1978a, 1978b), and Dodson and McClelland-Brown (1980) for noninteracting SDs. They point out that the treatment of Dodson and

McClelland-Brown (1980) differed by that of York (1978a) and York (1978b) by a factor of 2, owing to differences in the weak field approximation. They also expanded the treatment of rate dependence to heating as well as cooling and developed a novel way of measuring the frequency factor, C, directly. Over the years, this "constant" has been assumed to be 10^8/s by, for example, Stacey and Banerjee (1974) and 10^9/s by, for example, Halgedahl et al. (1980). Moskowitz et al. (1997) also experimentally determined a value of $\sim 10^9$/s. For comparison, the values of Berndt et al. (2017) ranged from 10^{13}/s to $\sim 10^9$/s. While Néel was fully aware that blocking occurs over a range of temperatures, he supposed that the range was quite small and adopted the approximation of a discrete blocking temperature. Berndt et al. (2017) found a range of temperatures of 5–20 K over which blocking takes place in practice.

Berndt and Muxworthy (2017) simulated TRM acquisition from Néel theory using a distribution of grain sizes and cooling times ranging from 10 min to a million years. Their calculations agreed well with those of Halgedahl et al. (1980), underscoring the possibility of up to 60% overestimates for field strength for slowly cooled rocks.

2.2. Non-SD Remanences

The situation becomes even more complicated when dealing with grains other than noninteracting SD. First of all, grains that are nominally SD behave differently if they intereact with neighboring SD grains. Shcherbakov et al. (1996) showed that in such populations, the dominant energies are not simply those within a single crystal, but instead the so-called "interaction" energy. How this will effect cooling rate however has not been explored.

Stacey (1963) predicted that MD grains would have the opposite effect than SD grains with MD TRMs being lower when more slowly cooled. He also surmised that so-called PSD grains would have an SD-like cooling rate effect, which could be used to distinguish them from MD grains. McClelland-Brown (1984) noted that the MD sample with a grain size range of 2.3–65 μm showed a decreased intensity for the slowly cooled experiment. Yu (2011) also tested PSD (1.06 μm) and MD (18.3 μm) magnetites and natural SD (Tudor Gabbro), PSD (basalts), and MD (granites) studied in previous publications. His natural PSD samples had estimates ranging from 11% underestimation to 18% overestimation, and while the synthetic and natural MD samples were both described as nonlinear, his data suggested that the slow-cooled experiments had lower TRMs than the fast-cooled experiments.

In a comprehensive review of the literature as well some additional experiments of their own, Biggin et al. (2013) concluded that the cooling rate effect for PSD, MD, or interacting SD grains is unlikely to exceed 10% (which they deemed "negligible"). And recently, Ferk et al. (2014) showed that small PSD grains had larger TRMs during slow cooling but the effect was negligible in larger PSD and MD grains.

Absent an analytical theory for PSD and MD grains, Winklhofer et al. (1997) performed 3-D micromagnetic modeling experiments to predict blocking temperatures for a range of magnetite particles. They suggested that fast cooling might result in a particular grain being blocked in an SD state, while during slow cooling, the same grain could be blocked in a vortex state, resulting in a considerable overestimation of the paleofield. Dunlop et al. (1994) and Muxworthy et al. (2003) explain the negative cooling rate effect in MD grains by nucleation of domain walls during cooling. Slower cooling allows more nucleation events, resulting in reduced magnetizations.

In a novel treatment of the cooling rate effect, Muxworthy et al. (2013) used a Preisach-based approach developed by Muxworthy et al. (2011) to estimate cooling rate corrections for slowly cooled rocks. Using FORC data, they developed a temperature dependent cooling rate correction that was up to 50% for the Modipe Gabbro whose remanence has a significant contribution for PSD grain sizes.

Two other processes could effect the dependence of magnetization on cooling rate: magnetic disaccommodation (Moskowitz, 1985) and reordering of cations and/or vacancies in the crystal structure Bowles and Jackson (2016). Both of these can occur below the Curie temperature and would be cooling rate dependent.

There is therefore little consensus of what the cooling rate dependence of TRM should be in even the simplest case of noninteracting SD grains (Dodson & McClelland-Brown, 1980, vs. Halgedahl et al., 1980). Furthermore, larger grain sizes should either have a small or even negative effect, yet experimental data for this grain size range are ambiguous. We therefore attempt to address the problem of cooling rate dependence in natural samples with a range of grain sizes. We selected suites of samples based on their behavior during Thellier-Thellier type experiments and subjected them to new experiments using a

Table 1
Locations, Lithologies, Age Ranges, and Citations of Samples Used in This Study

Locations	Lat. (°N)	Long. (°E)	Lithology	Age range	Citation DOI
McMurdo	−76.23	−167.43	Basalt	1.26–2.28 Ma	10.1029/2008GC002072
Socorro Island	18.78	−110.98	Peralkaline trachyte	0.35–0.55 Ma	10.1186/BF03352899
Hawaii	19.90	−155.58	Basalt	1843 CE	10.1016/j.pepi.2014.12.007
Jan Mayen	71.03	−8.29	Basalt	0.2–0.45 Ma	10.1002/ggge.20174
Costa Rica	9.93	−84.09	Basalt	<2 Ma	10.1002/ggge.20199

"fresh" laboratory-acquired thermal remanence in two cooling times (<1 and ~10 hr). We find that proxies for domain state based on hysteresis parameters do not predict cooling rate dependence or accuracy of paleointensity estimates.

3. Methods

3.1. Paleointensity Experiment

Studies of the paleosecular variation of the geomagnetic field by Lawrence et al. (2009), Cromwell et al. (2015), Sbarbori et al. (2009), Cromwell, Tauxe, et al. (2013), and Cromwell, Constable, et al. (2013) obtained samples from lava flows from Antarctica, Hawaii, Socorro Island, Jan Mayen, and Costa Rica, respectively (see Table 1). Samples from these studies were subjected to IZZI experiments (Yu et al., 2004) in the Scripps Institution of Oceanography paleomagnetics laboratory during the original investigations. Based on results from these original experiments (available in the MagIC database using the syntax https://earthref.org/MagIC/DOI/CITATIONDOI where the citation DOI is substituted in for CITATION-DOI), we selected specimens for reanalysis in the present study.

The IZZI method is a Königsberger-Thellier-Thellier (see Tauxe & Yamazaki, 2015, for a recent review) type experiment that replaces the original natural remanence magnetization (NRM) with a laboratory TRM. Data for the straight and curved sample sets are shown in Figures 1 and 2, respectively. The experimental protocol alternates steps that cool the specimen from a given temperature in the presence of a laboratory field (infield step, "I") with cooling in a zero field ("Z" steps) at increasing temperatures. The insets in the lower left-hand corners of the first two columns of Figures 1 and 2 show the progressive demagnetization of the NRM plotted as Zijderveld diagrams (Zijderveld, 1967). These show univectorial decay to the origin. The data shown in these figures are all in specimen coordinates and have not been corrected to geographic coordinates for the present purpose. The insets in the upper right-hand corners of the first two columns of Figures 1 and 2 show the progressive demagnetization of the NRM as blue dots and the acquisition of the laboratory TRM as red dots at each temperature step. The order of "infield-zerofield' and "zerofield-infield" heating steps switches with each subsequent heating step. In-field steps at lower temperatures (pTRM checks) are inserted within every zerofield-infield step to test if the capacity to acquire remanance of the specimen had changed. NRM remaining after each heating step is plotted against the pTRM gained in the so-called "Arai" plots (Nagata et al., 1963) shown in Figures 1 and 2.

Many of the original IZZI experiments "failed" the paleointensity selection criteria adopted by the authors but did not fail pTRM check tests for chemical alteration (see, e.g., Figures 1, column 1, and 2, column 1). The thermal stability of these samples allows us to repeat the IZZI experiments (although on different specimens) including repeated high-temperature treatment necessary for testing for a cooling rate dependence.

3.2. Domain State Proxies

As outlined in section 2, there is controversy over the dependence of the cooling rate effect on domain state; hence, we would like to characterize our specimens in terms of domain state. Many methods have been proposed in the literature for doing this, including the classic approach of Day et al. (1977) whereby several ratios of statistics are calculated from hysteresis loops, namely, the ratio of saturation remanence (M_r) to saturation magnetization (M_s) and the ratio of coercivity of remanence (H_{cr}) to coercivity (H_c). More recently, Paterson et al. (2017) proposed a slight modification of these ratios by combining them together into a single "bulk domain stability" (BDS) statistic. We calculate BDS of Paterson et al. (2017) using the relationship from their appendix.

$$BDS = -0.3900\left[\log\left(\frac{B_{cr}}{B_c}\right) - 0.6062\right] + 0.6353[\log\left(\frac{M_r}{M_s}\right) + 1.2018].$$

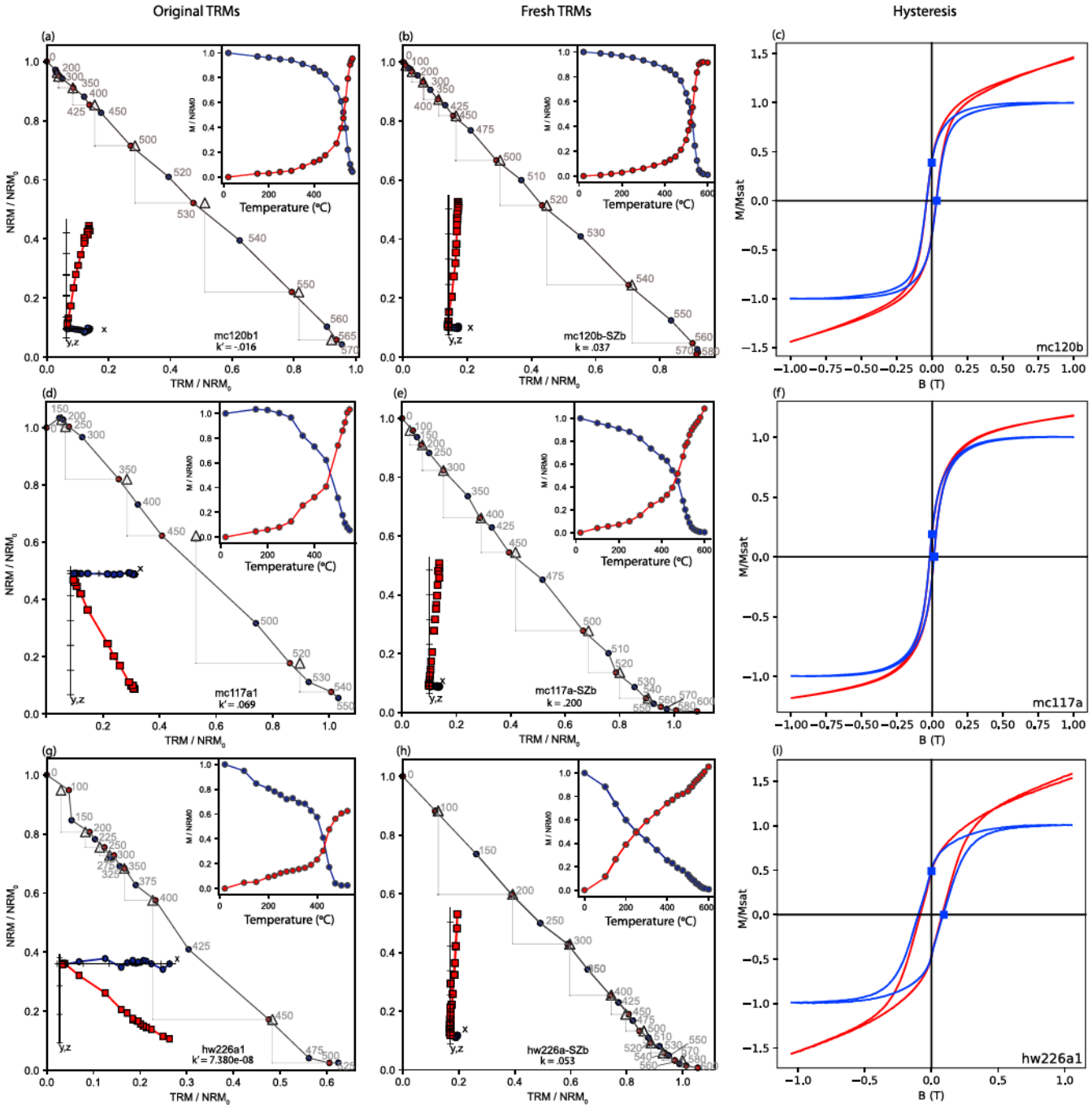

Figure 1. Column 1: (a, d, and g) representative Arai plots of straight samples from the original experiments. Red (blue) dots are the zerofield-infield (infield-zerofield) steps, and triangles are the pTRM check steps. A threshold value of 0.164 (Paterson, 2011; Paterson et al., 2014) for the absolute value of curvature (k'), calculated with a minimum FRAC of 0.78, was used as a threshold to distinguish between straight and curved behavior. Column 2: (b, e, and h) experiments on fresh TRMs. Symbols as in Column 1. k values calculated for the entire data set. Insets in columns 1 and 2 are as follows. Lower left corners: Zijderveld diagrams where components of the magnetization (normalized to NRM) are plotted for each demagnetization step. Blue dots are X, Y pairs, and red squares are X, Z pairs. Specimens are unoriented. Upper right corners: magnetization versus demagnetization temperature with NRM (blue circles) and pTRM gained (red circles), normalized by the initial NRM. Column 3: (c, f, and i) corresponding hysteresis plots of samples shown in columns 1 and 2. The red curve includes the nonferromagnetic (paramagnetic) contribution, and the blue curve is the resulting curve after subtraction of the paramagnetic slope.
TRM = thermal remanent magnetization; NRM = natural remanence magnetization.

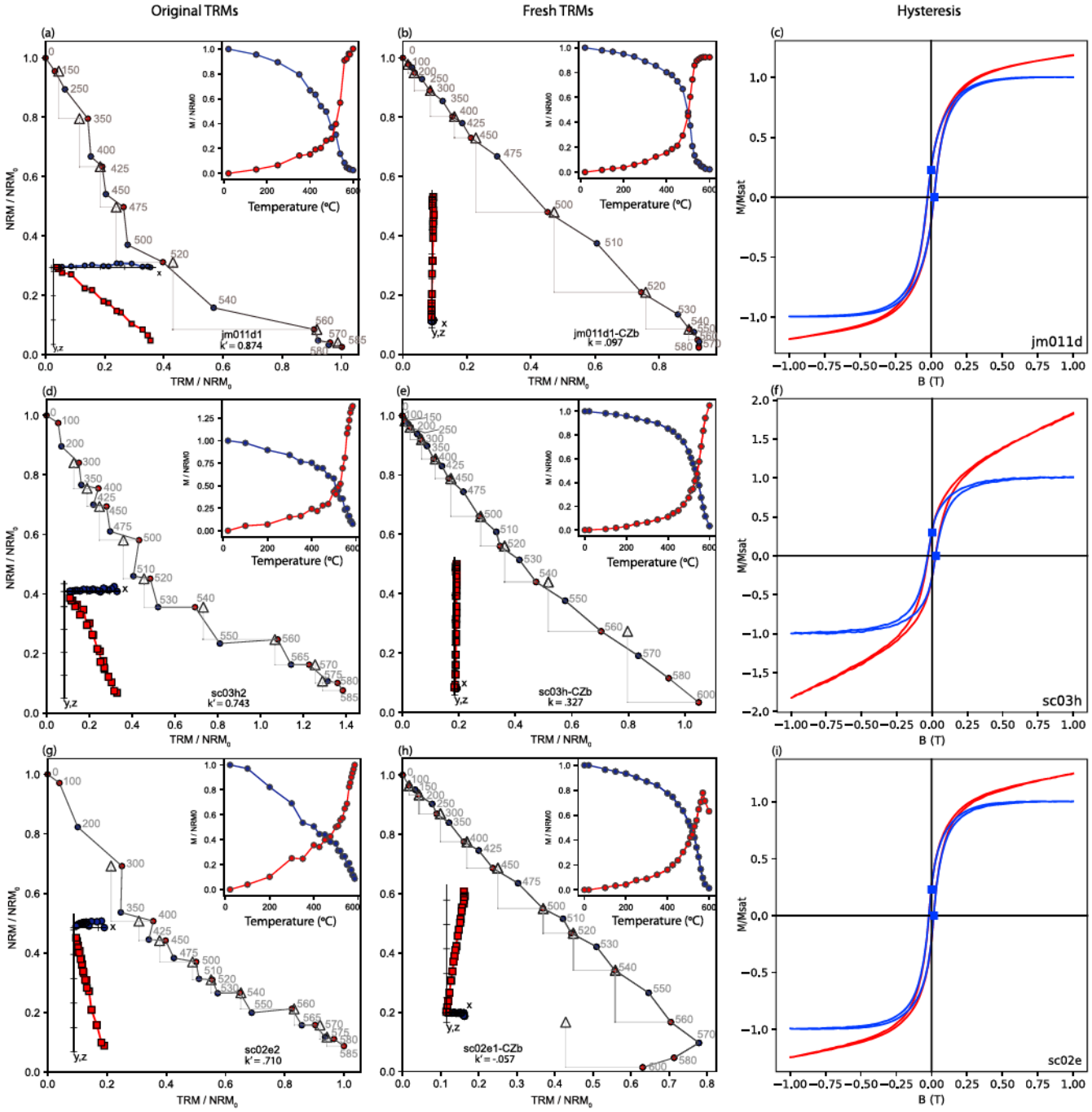

Figure 2. Same as Figure 1 but for curved samples with the exception of column (2h), which has a k' value calculated excluding the data from the last two temperature steps, as this specimen altered after reheating to 580°C. TRM = thermal remanent magnetization; NRM = natural remanence magnetization.

Using the values for $\frac{M_r}{M_s}$ and $\frac{B_{cr}}{B_c}$ or 0.5 and 1.5, respectively, for the SD/PSD transition of Day et al. (1977), we get a BDS value of 0.74 while values of 4 and 0.05 for the PSD/MD transition translate to a BDS value of 0.57. Note that Dunlop and Ozdemir (1997) point out that the choice of $\frac{B_{cr}}{B_c}$ ratio by Day et al. (1977) of 1.5 is arbitrary and can be between 1 and 2. Using a value of 1 instead yields a BSD of 0.81.

To characterize the samples in terms of hysteresis behavior, we measured hysteresis loops on a sister specimen (<30 mg) from each sample. These experiments were performed on a Micromag 2900 alternating gradient field magnetometer. Examples of hysteresis loops are shown in column 3 of Figures 1 and 2.

Paterson (2011) proposed a different way of assessing domain state by using the curvature of Arai plots. His "curvature" statistic k is the inverse of the radius of a unit circle that best fits the data in the Arai plot. A straight line on the Arai plot would have a k value of zero and that of a perfect downward bowed circle would be unity. Negative values imply upward bowed Arai plots, and values in excess of unity are more highly curved than a circle. Paterson (2011) suggested the threshold value of $k < 0.164$ as diagnostic of SD-like behavior and $k > 0.164$ for MD-like behavior. Strictly speaking, k is calculated using all of the data, including points at either end which may be deemed suspect based on failure of a pTRM test, or presence of a small viscous remanence, for example. We therefore used the curvature statistic k' of Paterson et al. (2014), which is the value of k for the measurements actually used in the slope calculation. This, combined with a high value for FRAC (the fraction of remanence used in the slope calculation as defined by Paterson et al., 2014), protects against using only a small fraction of the data. Here we calculated the k' statistic for the original experiments using a FRAC of 0.78. Higher values for FRAC were in many cases not possible as the original experiments did not always continue to the maximum blocking temperature. We used the threshold value of 0.164 for k' to separate samples into two broad categories: those with straight Arai plots ($k' < 0.164$; Figure 1, column 1) and those with curved Arai plots ($k' > 0.164$; Figure 2, column 1). For the present study we chose a total of 24 samples with 12 in each category from the original sample collection with k' values ranging from −0.42 to 1.69.

We prepared specimens from the 24 original samples by cementing small chips (~30 mg) into a borosilicate glass tube using Whatman filter paper and KaSil glue. These were then thermally demagnetized in a laboratory oven at 580 °C. Following this, the specimens were given a new laboratory controlled total TRM by cooling from 600 °C in a 70 μT field aligned parallel to the specimen $-z$ direction. These fresh TRMs were subjected to an IZZI experiment (see examples in column 2 of Figures 1 and 2). After completion of the IZZI experiments on the fresh TRMs, the specimens were given total TRMs as before but cooled at two different rates (calculated using the method of Shaar & Tauxe, 2013): "fast" (43.6 K/min) and "slow" (1.3 K/min). The fast-cooling step was repeated after the slow-cooling step to check for alteration. None was detected.

We analyzed our IZZI experimental data with the Thellier GUI program of Shaar and Tauxe (2013) and hysteresis loops with hysteresis_magic.py, both in the PmagPy software package of Tauxe et al. (2016), available at https://github.com/PmagPy/PmagPy. For the analysis described here, intensity and curvatures were calculated using all of the data with one exception. For specimen sc02e1-CZB, temperature steps from 0° to 580° were used with a FRAC value of 0.96 because this specimen altered (sc02e1) after heating to 580°. In this single case, k' was calculated instead of k. Values for k (k') in the fresh experiments ranged from −.06 (slightly bowed upward) to 0.329 (significantly curved downward). Intensity estimates ranged from 66.8 to 82.4 μT.

4. Results

4.1. Domain State Proxies

We calculated saturation remanence, M_r, saturation magnetization, M_s, coercivity of remanence, B_{cr}, and coercivity, B_c, from the hysteresis loops. We plot the ratios M_r/M_s (squareness) and B_{cr}/B_c in a Day plot (Day et al., 1977) in Figure 3a, the squareness versus coercivity (Néel, 1955) in Figure 3b and a log-log version of the Day plot in Figure 3c, along with the so-called BDS line (in black) of Paterson et al. (2017). In general, all of the data plot well above the theoretical SD-MD mixing line of Dunlop (2002) and Dunlop and Carter-Stiglitz (2006), underscoring the difficulty in using Day plots to characterize samples in terms of domain state as pointed out by Roberts et al. (2018). However, although there is considerable overlap on the Day plot, the hysteresis data from the straight sample set (squares) have higher squareness values than those from the curved set (circles). Similarly, the data from the straight sample set plot above the trend of the curved samples in the squareness versus coercivity plot (Figure 3b). Higher squareness values indicate that the magnetic remanence of individual magnetic grains is closer to the saturation magnetization, a behavior often used to argue for greater simplicity of domain structures (SD vs., say, MD).

4.2. Paleointensity

Figures 4a and 4b compare the difference in the k' statistic between the original experiments and k calculated for the fresh TRMs for the two groups of samples (straight and curved). The results fall into five categories.

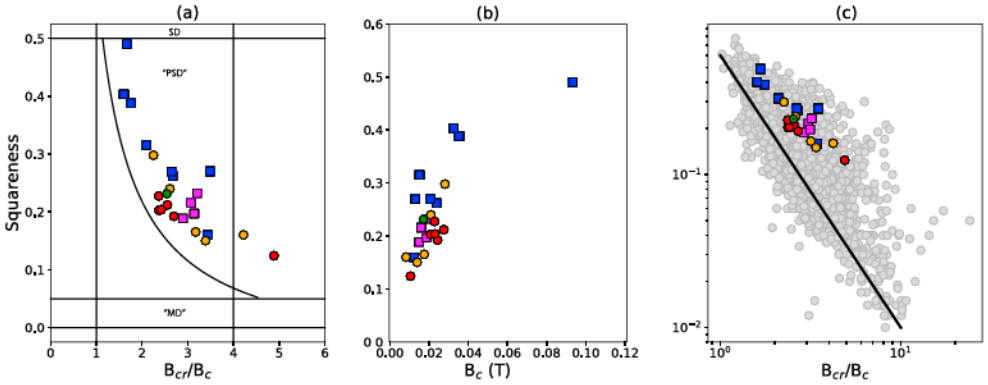

Figure 3. (a) "Day" plot (Day et al., 1977) of straight (blue and magenta squares) and curved (red, orange, and green circles) specimens. Solid line is SD-MD mixing curve of Dunlop (2002) and Dunlop and Carter-Stiglitz (2006); see Tauxe et al. (2010). (b) Plot of squareness (M_r/M_s) against coercivity (B_c). Symbols as in (a). (c) Log-log plot of data in (a) and geological hysteresis data from Paterson et al. (2017), gray dots. Black line is the bulk domain stability trend from Paterson et al. (2017). PSD = pseudo single domain; SD = single domain; MD = multidomain.

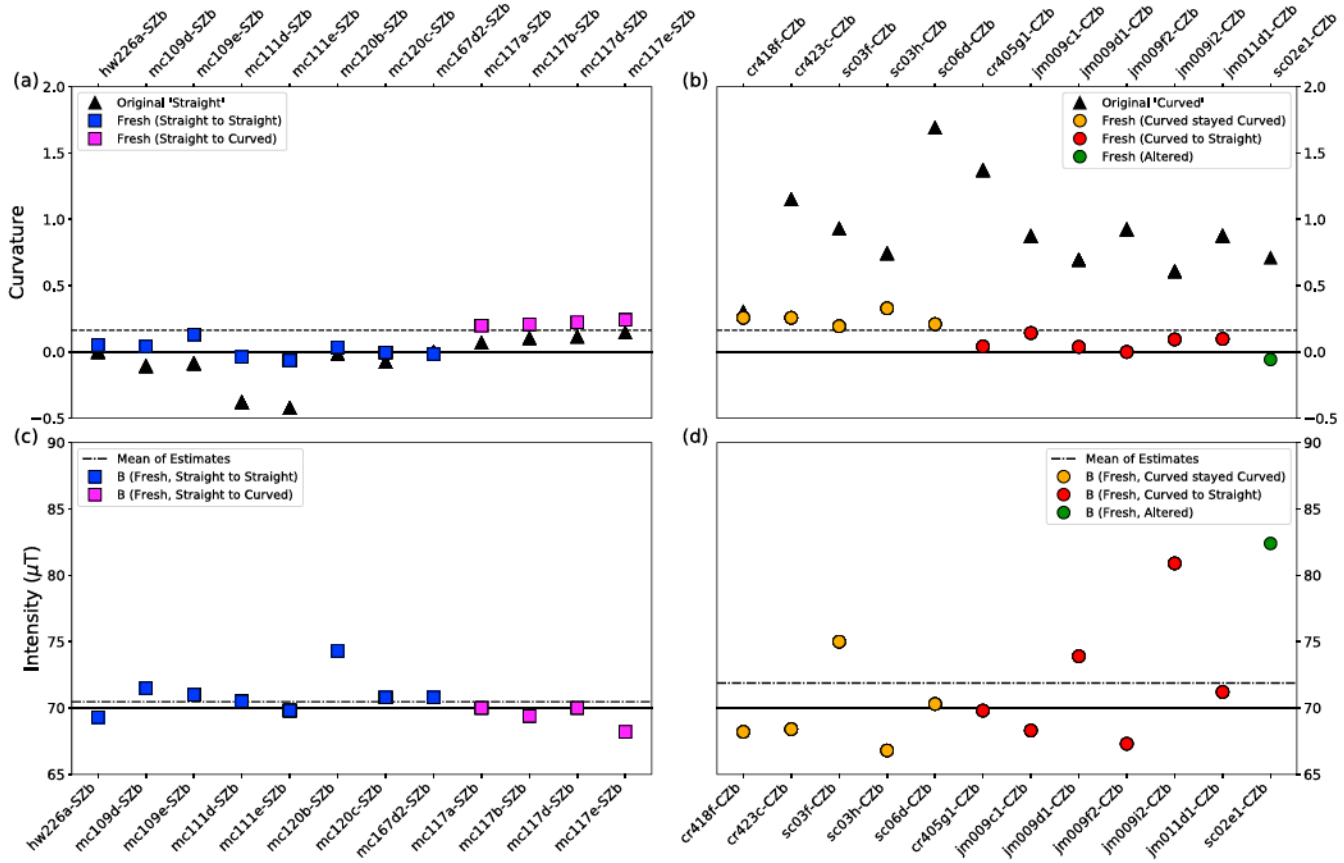

Figure 4. (a and b) Curvatures (k') from the original experiments (black triangles) versus the k, (k') values those derived from the fresh thermal remanent magnetizations (colored squares and circles for straight and curved experiments, respectively). Dashed line is the 0.164 bound for straight ($k' < 0.164$) and curved ($k' > 0.164$) Arai plots. Specimen names with "S" in them (a and c) were categorized as straight and those with "C" (b and d) were curved. (c and d) Estimated paleointensities from fresh thermal remanent magnetizations acquired in a 70 μT field. Mean values of each group of specimens are shown as dashed-dot lines.

Table 2
Data Table for All Specimens

Specimen	Original k'	Fresh k	M_{slow}/M_{fast}	M_r/M_s	BDS	Intensity (μT)	Marker color
			Straight				
hw226a-SZb	0.000	0.053	1.065	0.49	0.72	69.3	Blue
mc109d-SZb	−0.107	0.042	1.049	0.26	0.46	71.5	Blue
mc109e-SZb	−0.087	0.131	1.058	0.27	0.43	71.0	Blue
mc111d-SZb	−0.379	−0.037	1.027	0.32	0.57	70.5	Blue
mc111e-SZb	−0.423	−0.064	1.037	0.27	0.47	69.8	Blue
mc120b-SZb	−0.016	−0.004	1.032	0.39	0.64	74.3	Blue
mc120c-SZb	−0.076	−0.003	1.018	0.40	0.67	70.8	Blue
mc167d2-SZb	0.000	−0.016	1.082	0.16	0.29	70.8	Blue
mc117a-SZb	0.069	0.199	0.969	0.19	0.36	70.0	Magenta
mc117b-SZb	0.103	0.209	0.966	0.22	0.39	69.4	Magenta
mc117d-SZb	0.115	0.224	0.981	0.20	0.36	70.0	Magenta
mc117e-SZb	0.145	0.242	0.999	0.23	0.40	68.2	Magenta
			Curved				
cr418f-CZb	0.302	0.258	1.046	0.15	0.27	68.2	Orange
cr423c-CZb	1.150	0.258	1.011	0.17	0.31	68.4	Orange
sc03f-CZb	0.929	0.194	1.019	0.24	0.44	75.0	Orange
sc03h-CZb	0.743	0.329	1.039	0.30	0.53	66.8	Orange
sc06d-CZb	1.689	0.210	1.015	0.16	0.25	70.3	Orange
cr405g1-CZb	1.370	0.042	1.040	0.12	0.16	69.8	Red
jm009c1-CZb	0.873	0.143	1.105	0.19	0.38	68.3	Red
jm009d1-CZb	0.694	0.038	1.068	0.20	0.41	73.9	Red
jm009f2-CZb	0.923	0.000	1.115	0.21	0.41	67.3	Red
jm009i2-CZb	0.607	0.095	1.053	0.20	0.41	80.9	Red
jm011d1-CZb	0.874	0.098	1.061	0.23	0.45	71.2	Red
sc02e1-CZb*	0.710	−0.057	[0.958]	0.23	0.44	82.4	Green

Note. BDS = bulk domain stability. Value for curvature was k' as opposed to k (see text).

1. The majority of the straight samples retained low k values ($k < 0.164$) in the second heating experiment (blue squares in Figure 4a). Four of the 12 specimens (all from the same lava flow mc117) became slightly more curved in the second TRM experiment.
2. The k values of all four mc117 samples were larger in the second experiment (magenta squares in Figure 4a) and slightly surpassed the critical $k < 0.164$ value. After the second heating experiment, a slight curvature can be seen on the Arai diagrams (e.g., Figure 1e) in the higher temperature heating steps (>560 °C). It is unknown whether this curvature would have been present in the original experiment because the highest temperature step implemented was 550 °C.
3. All 12 specimens of the originally curved samples became straighter after the second heating experiment with six of the specimens falling within the $k = \pm 0.164$ bounds (red circles in Figure 4b). This could be the result of disaccommodation or reordering (Bowles & Jackson, 2016; Moskowitz, 1985). These effects would be much slower in the original cooling than in the laboratory experiment, which would affect the curvature of the Arai plot.
4. Five of the 12 curved specimens, while straighter in the fresh experiments, had k values exceeding the 0.164 threshold (orange circles in Figure 4b).
5. One notable exception is the negative k' value calculated for sc02e1 (green rimmed, white circle). The original Arai diagram for this sample featured a concave down and "zig-zagged" curve (Figure 2d). In the second experiment, the Arai diagram was much straighter until reaching the temperature steps above

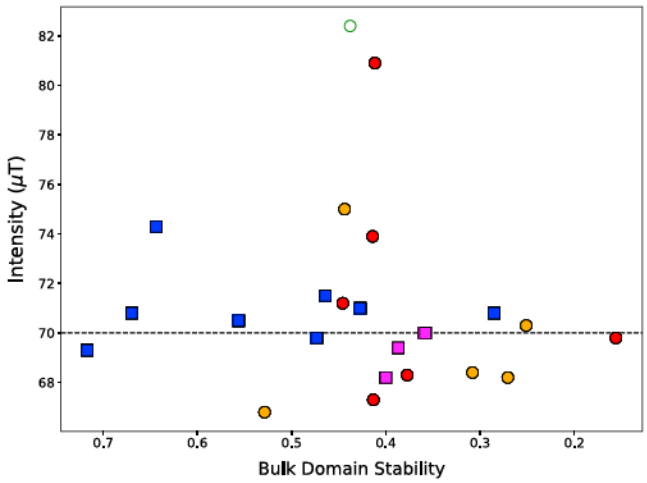

Figure 5. Intensity estimate from Figure 4 versus sample bulk domain stability values (Figure 3c), calculated as in Paterson et al. (2017). Symbols as in Figure 4.

570 °C, where a hook-like feature is observed, changing the sign of the k' value. We attribute this behavior to alteration of this trachytic specimen, as seen in the pTRM check step at 560 °C (white triangle in Figure 2h).

Regardless of the change in curvature from the original to the "fresh TRM" heating experiments, Figures 4c and 4d show that the estimated "paleointensities" calculated from each specimen have a much more significant scatter among the originally curved samples compared with the originally straight samples (Table 2). The straight set had interpretations ranging from 68.2 to 74.3 with a mean and standard deviation of 70.5 ± 1.5 μT while the curved set ranged from 66.2 to 82.4 with a mean of 71.9 ± 5.2 μT.

Paterson et al. (2017) suggested the use of BDS, a function of M_r/M_s, and B_{cr}/B_c as a guide to interpreting paleointensity data. They found a relationship between performance in a paleointensity experiment and BDS

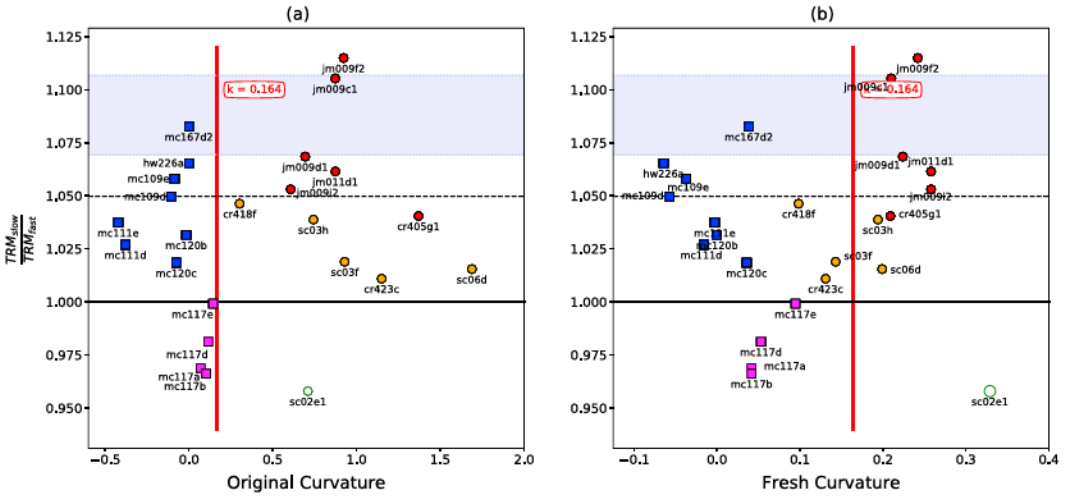

Figure 6. Ratio of TRM acquired during slow cooling (1.6 K/min) to fast cooling (43.6 K/min), plotted against curvature (k). The value expected from single-domain theory is shown as a dashed line. (a) Calculated from the "original" experiments. (b) Calculated from the fresh experiments. Blue and magenta squares show originally straight specimens and red, orange, and hollow green circles show originally curved specimens. Each color represents an assigned category based on its observed experimental behavior. The hollow green circle altered during the experiment. The red vertical line is $k = 0.164$, a theoretical critical value separating SD-like behavior from MD-like remanences (Paterson, 2011). Dashed lines are the mean value of the $\frac{TRM_{slow}}{TRM_{fast}}$ values greater than unity and the lavender boxes are the range predicted from Néel (1949) theory by Halgedahl et al. (1980) and Dodson and McClelland-Brown (1980). TRM = thermal remanent magnetization; SD = single domain; MD = multidomain.

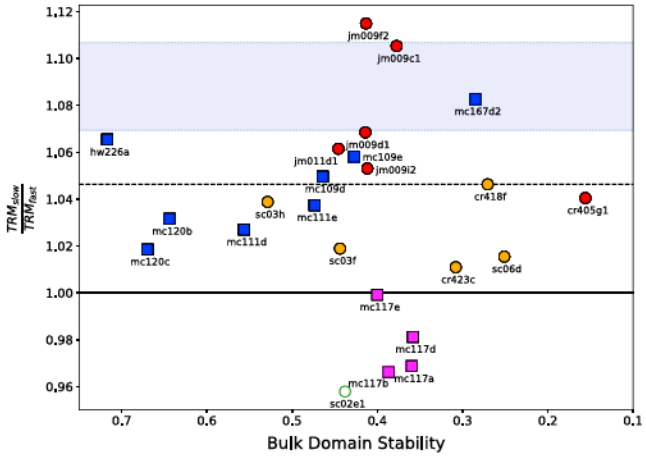

Figure 7. Cooling rate ratio plotted against bulk domain stability. Symbols, dashed lines, and lavender box same as in Figure 6. TRM = thermal remanent magnetization.

whereby specimens with higher BDS values performed more accurately than those with lower BDS values. In our experiments (Figure 5), we find no clear relationship between paleointensity accuracy and BDS.

4.3. Cooling Rate

Figures 6 and 7 show the results of our cooling rate experiments. In addition to changes in curvature, we found a significant cooling rate dependence for nearly all curvatures (Figure 6a,b). The specimens with the highest cooling rate dependence (jm009f2 and jm009c1) had original curvature values significantly higher than the cutoff value of 0.164 recommended by Paterson (2011; Figure 6a). However, the curvature in the fresh TRM experiment was below the cutoff. The cooling rates of cr418f and sc03h, whose curvatures in both the original and fresh TRM experiments were higher than the cutoff, had cooling rates near those predicted for SD behavior. Three specimens have negative cooling rates, which many studies have predicted for MD behavior (e.g., Dunlop et al., 1994; Muxworthy et al., 2003; Stacey, 1963). These specimens were from lava flow mc117 and had straight original curvatures but became slightly more curved in the fresh experiments.

We plot the cooling rate dependence from Figure 6 against BDS in Figure 7. The samples with the highest and lowest cooling rate dependencies all have similar (moderate) BDS values of around 0.4 with no clear relationship between the two parameters.

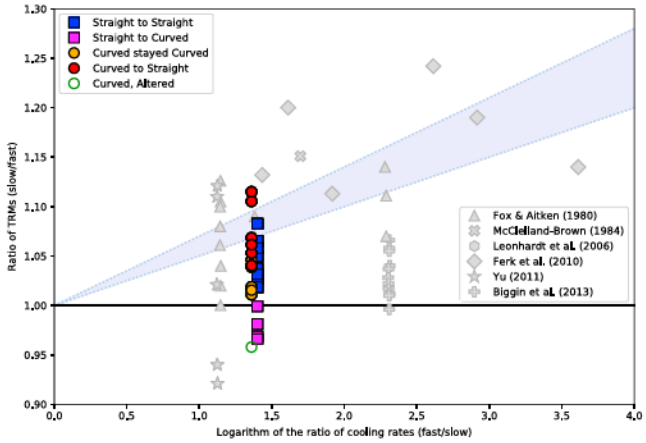

Figure 8. The light blue band is the theoretical predictions of Halgedahl et al. (1980) and Dodson and McClelland-Brown (1980), lower and upper bounds of shaded polygon, respectively. Colored circles and squares (offset for clarity) are data from this study; same symbols as previous figures. Gray symbols are a compilation of previously published data, as cited in section 2. TRM = thermal remanent magnetization.

5. Discussion

As discussed in section 2, there is little consensus in the literature regarding cooling rate dependence versus domain state. We plot empirical cooling rate dependencies found in various studies as gray symbols in Figure 8 along with the theoretical predictions of Halgedahl et al. (1980) and Dodson and McClelland-Brown (1980) for SD grains. In this paper we examined a variety of natural specimens with a range of parameters generally regarded as proxies for domain state, including curvature of the Arai plots and hysteresis ratios. As described in section 4, we find no consistent pattern of cooling rate dependence versus domain state proxy. We plot the data in Figure 8 as colored symbols, and ironically, it seems that the largest cooling rate dependence is found in the curved sample set (colored circles) while the straight sample set lower or even a negative cooling rate dependence. It appears that cooling rate cannot be neglected for non-SD material and that the theoretical predictions can likely not be extrapolated out to very long cooling rates. We recommend that cooling rate dependence be measured, unless the laboratory and natural cooling rates are similar (as for basaltic glasses, Bowles et al. (2005)).

All of the originally straight samples were specifically chosen because they were rapidly cooled in nature resulting in fine grained, even glassy textures. In the original studies, no cooling rate corrections were applied because the original and laboratory cooling rates are quite similar. Interpretations from the curved samples were not considered reliable in the original studies, so no consideration of cooling rate was given. Here we find that although the paleointensity results are certainly more scattered for the curved samples, the average of the 12 estimates was quite accurate. In other words, there does not appear to be a consistent bias, and if a sufficient number of specimens are included in the analysis, an accurate result (although less precise) can be estimated. However, cooling rate must be taken into account, as it cannot be assumed to be negligible.

6. Conclusions

1. We divided a set of 24 paleomagnetic samples previously analyzed for paleointensity into two groups based on the curvature of their Arai plots. One group had straight NRM versus TRM plots frequently considered "ideal" in paleointensity studies, and the other had curved plots using the curvature criterion k' of 0.164 that Paterson et al. (2012) recommended as a means to separate SD behavior from MD. A total of 12 specimens from each of the straight and curved sample sets were given a fresh TRM in a laboratory field of 70 μT and the paleointensity experiment was repeated. The fresh TRMs often behaved differently than in the original experiments. All experiments on fresh TRMs of the originally curved sample set were much straighter with seven of the 12 having curvatures less than 0.164 threshold value. Four specimens from the straight group, all from the same lava flow, became slightly more curved.
2. Extremely accurate and precise intensities were recovered from the straight sample set with a range in estimates from 68.2 to 74.3 μT. The curved sample set was much more scattered with results ranging from 66.8 to 82.4 μT. Nonetheless, the average values of the two sets (70.1 and 71.9 μT) were quite close to the laboratory field of 70 μT.
3. A cooling rate dependence of TRM for SD remanences is expected from Néel theory (Néel, 1949), whereas larger grain sizes (so-called PSD) are widely thought to have a negligible effect (e.g., Biggin et al., 2013; Ferk et al., 2014; Yu, 2011). Apart from the four specimens that were originally straight but became more curved in the fresh TRM experiments (with zero to negative cooling rate dependences), the remaining 20 specimens, regardless of apparent domain state, had a cooling rate dependence of TRM ranging from near zero to ~12%.
4. We performed hysteresis experiments on sister specimens from all samples, calculating the ratios of saturation remanence to saturation and coercivity of remanence to coercivity. From these, we calculated the BDS index of Paterson et al. (2017), which they claim is a proxy for domain state. BDS estimates and other hysteresis parameters proved to have little predictive value for paleointensity behavior. However, curvature proved to be highly correlated with both precision of the paleointensity estimates (with higher curvature leading to higher scatter in the results) and to be related to cooling rate dependence (with higher curvature associated with lower cooling rate (or even negative cooling rate) dependence.

Acknowledgments
We have benefited from discussions with Ron Shaar, Jeff Gee, Cathy Constable, Pat Castillo, Hanna Asefaw, Shelby Jones-Cervantes, Brendan Cych, Shuhui Cai, Wyn Williams, and Les Nagy. We are also grateful for help from Gabriel Santos for his design contributions and Carlos Anguiano for his lab assistance. The manuscript was significantly improved by the comments of the reviewers Ramon Egli and Adrian Muxworthy. This material is based upon work supported by the National Science Foundation under Grants EAR1547263 and EAR1827263. All measurement data related to this work will be available in the MagIC database upon acceptance of the manuscript (https://earthref.org/MagIC/DOI/2018GC007946).

References

Ben-Yosef, E., Tauxe, L., & Levy, T. (2010). Archaeomagnetic dating of copper smelting site F2 in the Timna Valley (Israel) and its implications for the modelling of ancient technological developments. *Archaeometry*, *52*, 110–1121. https://doi.org/10.1111/j.1475-4754.2010.00528

Berndt, T., & Muxworthy, A. (2017). Paleomagnetic field reconstruction from mixtures of titanomagnetites. *Earth and Planetary Science Letters*, *465*, 70–81. https://doi.org/10.1016/j.epsl.2017.02.033

Berndt, T., Paterson, G., Cao, C., & Muxworthy, A. (2017). Experimental test of the heating and cooling rate effect on blocking temperatures. *Geophysical Journal International*, *210*, 255–269. https://doi.org/10.1093/gji/ggx153

Biggin, A., Badejo, S., Hodgson, E., Muxworthy, A., Shaw, J., & Dekkers, M. (2013). The effect of cooling rate on the intensity of thermoremanent magnetization (TRM) acquired by assemblages of pseudo-single domain, multidomain and interacting single-domain grains. *Geophysical Journal International*, *193*, 1239–1249. https://doi.org/10.1093/gji/ggt078

Biggin, A., Steinberger, B., Aubert, J., Suttie, N., Holme, R., Torsvik, T. H., et al. (2012). Possible links between long-term geomagnetic variations and whole-mantle convection processes. *Nature Geoscience*, *5*, 526–533.

Bowles, J., Gee, J. S., Kent, D., Bergmanis, E., & Sinton, J. (2005). Cooling rate effects on paleointensity estimates in submarine basaltic glass and implications for dating young flows. *Geochemistry, Geophysics, Geosystems*, *6*, Q07002. https://doi.org/10.1029/2004GC000900

Bowles, J. A., & Jackson, M. J. (2016). Effects of titanomagnetite reordering processes on thermal demagneitzaiton and paleointensity experiments. *Geochemistry, Geophysics, Geosystems*, *17*, 4848–4858. https://doi.org/10.1002/2016GC006607

Cromwell, G., Constable, C., Staudigel, H., Tauxe, L., & Gans, P. (2013). Revised and updated paleomagnetic results from Costa Rica. *Geochemistry, Geophysics, Geosystems*, *14*, 3379–3388. https://doi.org/10.1002/ggge.20199

Cromwell, G., Tauxe, L., Staudigel, H., Constable, C., Koppers, A., & Pedersen, R.-B. (2013). In search of long-term hemispheric asymmetry in the geomagnetic field: Results from high northern latitudes. *Geochemistry, Geophysics, Geosystems*, *14*, 3234–3249. https://doi.org/10.1002/ggge.20174

Cromwell, G., Tauxe, L., Staudigel, H., & Ron, H. (2015). Paleointensity estimates from historic and modern Hawaiian lava flows using basaltic volcanic glass as a primary source material. *Physics of the Earth and Planetary Interiors*, *241*, 44–56.

Day, R., Fuller, M. D., & Schmidt, V. A. (1977). Hysteresis properties of titanomagnetites: Grain size and composition dependence. *Physics of the Earth and Planetary Interiors*, *13*, 260–266.

Dodson, M., & McClelland-Brown, E. (1980). Magnetic blocking temperatures of single-domain grains during slow cooling. *Journal of Geophysical Research*, *85*(B5), 2625–2637.

Dunlop, D. J. (2002). Theory and application of the Day plot (Mrs/Ms versus Hcr/Hc) 1. Theoretical curves and tests using titanomagnetite data. *Journal of Geophysical Research*, *107*(B3), 2056. https://doi.org/10.1029/2001JB000486

Dunlop, D. J. (2011). Physical basis of the Thellier-Thellier and related paleointensity methods. *Physics of the Earth and Planetary Interiors*, *187*, 118–138.

Dunlop, D. J., & Carter-Stiglitz, B. (2006). Day plots of mixtures of superparamagnetic, single-domain, pseudosingle-domain, and multidomain magnetites. *Journal of Geophysical Research*, *111*, B12S09. https://doi.org/10.1029/2006JB004499

Dunlop, D., Newell, A., & Enkin, R. J. (1994). Transdomain thermoremanent magnetization. *Journal of Geophysical Research*, *99*(B10), 19,741–19,755. https://doi.org/10.1029/94JB01476

Dunlop, D., & Ozdemir, O. (1997). *Rock magnetism: Fundamentals and frontiers, Cambridge studies in magnetism*. New York: Cambridge University Press.

Ferk, A., Aulock, F. W. V., Leonhardt, R., Hess, K.-U., & Dingwell, D. B. (2010). A cooling rate bias in paleointensity determination from volcanic glass: An experimental demonstration. *Journal of Geophysical Research*, *115*, B08102. https://doi.org/10.1029/2009JB006964

Ferk, A., Leonhardt, R., Hess, K. U., Koch, S., Egli, R., Krasa, D., & Dingwell, D. (2014). Influence of cooling rate onthe thermoremanence of magnetite grains: Identifying the role of different magnetic domain states. *Journal of Geophysical Research: Solid Earth*, *119*, 1599–1606. https://doi.org/10.1002/2013JB010845

Fox, J. M. W., & Aitken, M. J. (1980). Cooling-rate dependence of thermoremanent magnetization. *Nature*, *283*, 462–463.

Halgedahl, S., Day, R., & Fuller, M. (1980). The effect of cooling rate on the intensity of weak-field TRM in single-domain magnetite. *Journal of Geophysical Research*, *85*(B7), 3690–3698.

Lawrence, K. P., Tauxe, L., Staudigel, H., Constable, C., Koppers, A., McIntosh, W. C., & Johnson, C. L. (2009). Paleomagnetic field properties near the Southern Hemisphere tangent cylinder. *Geochemistry, Geophysics, Geosystems*, *10*, Q01005. https://doi.org/10.1029/2008GC00207

McClelland-Brown, E. (1984). Experiments on TRM intensity dependence on cooling rate. *Geophysical Research Letters*, *11*(3), 205–208.

Mitra, R., Tauxe, L., & Gee, J. (2011). Detecting uniaxial single domain grains with a modified IRM technique. *Geophysical Journal International*, *187*, 1250–1258. https://doi.org/10.1111/j.1365-246X.2011.05224.x

Moskowitz, B. M. (1985). Magnetic viscosity, diffusion affer effect and disacomodation in natural and synthetic samples. *Geophysical Journal International*, *82*, 143–161.

Moskowitz, B. M., Frankel, R. B., Walton, S. A., Dickson, D., Wong, K. K. W., Douglas, T., & Hann, S. (1997). Determination of the pre-exponential frequency factor for superparamagnetic maghemite particles in magnetoferritin. *Journal of Geophysical Research*, *102*(B10), 22,671–22,680.

Muxworthy, A. R., Dunlop, D. J., & Williams, W. (2003). High-temperature magnetic stability of small magnetite particles. *Journal of Geophysical Research*, *108*(B5), 2281. https://doi.org/10.1029/2002JB00219

Muxworthy, A., Evans, M., Scourfield, S., & King, J. (2013). Paleointensity results from the late-Archaen Modipe Gabbro of Botswana. *Geochemistry, Geophysics, Geosystems*, *14*, 2198–2205. https://doi.org/10.1002/ggge.20142

Muxworthy, A. R., Heslop, D., Paterson, D., & Michalk, G. (2011). A Preisach method for estimating absolute paleofield intensity under the constraint of using only isothermal measurements: 2) Experimental testing. *Journal of Geophysical Research*, *116*, B04103. https://doi.org/10.1029/2010JB007844

Nagata, T., Arai, Y., & Momose, K. (1963). Secular variation of the geomagnetic total force during the last 5000 years. *Journal of Geophysical Research*, *68*(18), 5277–5281.

Néel, L. (1949). Théorie du trainage magnétique des ferromagnétiques en grains fines avec applications aux terres cuites. *Annales Geophysicae*, *5*, 99–136.

Néel, L. (1955). Some theoretical aspects of rock-magnetism. *Advances in Physics*, *4*, 191–243.

Newell, A. (2017). Frequency dependence of susceptibility in magnets with uniaxial and triaxial anisotropy. *Journal of Geophysical Research: Solid Earth*, *122*, 7544–7561. https://doi.org/10.1002/2017JB014176

Paterson, G. A. (2011). A simple test for the presence of multidomain behavior during paleointensity experiments. *Journal of Geophysical Research*, *116*(B10104). https://doi.org/10.1029/2011JB008369

Paterson, G., Biggin, A., Yamamoto, Y., & Pan, Y. X. (2012). Towards the robust selection of Thellier-type paleointensity data: The influence of experimental noise. *Geochemistry, Geophysics, Geosystems*, *13*, Q05Z43. https://doi.org/10.1029/2012GC004046

Paterson, G., Muxworthy, A., Yamamoto, Y., & Pan, Y. (2017). Bulk magnetic domain stability controls paleointensity fidelity. *Proceedings of the National Academy of Sciences of the United States of America*, *114*, 13,120–13,125. https://doi.org/10.1073/pnas.1714047114

Paterson, G., Tauxe, L., Biggin, A., Shaar, R., & Jonestrask, L. (2014). On improving the selection of Thellier-type paleointensity data. *Geochemistry, Geophysics, Geosystems*, *15*, 1180–1192. https://doi.org/10.1002/2013GC005135

Roberts, A., Tauxe, L., Heslop, D., Zhao, X., & Jiang, Z. (2018). A critical appraisal of the 'Day' Diagram. *Journal of Geophysical Research: Solid Earth*, *123*, 2618–2644. https://doi.org/10.1002/2017JB015247

Sbarbori, E., Tauxe, L., Gogichaishvili, A., Urrutia-Fucugauchi, J., & Bohrson, W. (2009). Paleomagnetic behavior of volcanic rocks from Isla Socorro, Mexico. *Earth Planets and Space*, *61*, 191–204.

Selkin, P., Gee, J., Tauxe, L., Meurer, W., & Newell, A. (2000). The effect of remanence anisotropy on paleointensity estimates: A case study from the Archean Stillwater complex. *Earth and Planetary Science Letters*, *182*, 403–416.

Shaar, R., & Tauxe, L. (2013). Thellier GUI: An integrated tool for analyzing paleointensity data from Thellier-type experiments. *Geochemistry, Geophysics, Geosystems*, *14*, 677–692. https://doi.org/10.1002/ggge.20062

Shcherbakov, V. P., Sycheva, N., & Lamash, B. E. (1996). Monte Carlo modelling of TRM and CRM acquisition and comparison of their properties in an ensemble of interacting SD grains. *Geophysical Research Letters*, *23*(20), 2827–2830.

Stacey, F. D. (1963). The physical theory of rock magnetism. *Advances in Physics*, *12*, 45–133.

Stacey, F. D., & Banerjee, S. K. (1974). *The Physical Principles of rock magnetism, developments in solid Earth geophysics* (Vol. 5). Amsterdam: Elsevier Sci. Publ. Co.

Tauxe, L., Banerjee, S. K., Butler, R., & van der Voo, R. (2010). *Essentials of paleomagnetism*. Berkeley: University of California Press.

Tauxe, L., Shaar, R., Jonestrask, L., Swanson-Hysell, N., Minnett, R., Koppers, A. A. P., et al. (2016). PmagPy: Software package for paleomagnetic data analysis and a bridge to the Magnetics Information Consortium (MagIC) Database. *Geochemistry, Geophysics, Geosystems*, *17*, 2450–2463. https://doi.org/10.1002/2016GC006307

Tauxe, L., & Yamazaki, T. (2015). Paleointensities (2nd ed.). In M. Kono et al. (Eds.), *Geomagnetism, treatise on geophysics* (Vol. 5, pp. 461–509). Amsterdam: Elsevier.

Thellier, E. (1938). Sur l'aimantation des terres cuites et ses applications géophysique. *Annales de l'Institut de Physique du Globe de Paris*, *16*, 157–302.

Thellier, E., & Thellier, O. (1959). Sur l'intensité du champ magnétique terrestre dans le passé historique et géologique. *Annales Geophysicae*, *15*, 285–378.

Wernsdorfer, W., Orozco, E. B., Hasselbach, K., Benoit, A., Barbara, B., Demoncy, N., et al. (1997). Experimental evidence of the Néel-Brown model of magnetization reversal. *Physical Review Letters*, *78*, 1791–1794.

Winklhofer, M., Fabian, K., & Heider, F. (1997). Magnetic blocking temperatures of magnetite calculated with a three-dimensional micromagnetic model. *Journal of Geophysical Research*, *102*(B10), 22,695–22,709.

York, D. (1978a). A formula describing both magnetic and isotopic blocking temperatures. *Earth and Planetary Science Letters*, *39*, 89–93.

York, D. (1978b). Magnetic blocking temperature. *Earth and Planetary Science Letters*, *39*, 94–97.

Yu, Y. (2011). Importance of cooling rate dependence of thermoremanence in paleointensity determination. *Journal of Geophysical Research*, *116*, B09101. https://doi.org/10.1029/2011JB008388

Yu, Y., Tauxe, L., & Genevey, A. (2004). Toward an optimal geomagnetic field intensity determination technique. *Geochemistry, Geophysics, Geosystems*, *5*, Q02H07. https://doi.org/10.1029/2003GC000630

Zijderveld, J. D. A. (1967). A. C. demagnetization of rocks: Analysis of results. In S. K. Runcorn et al. (Eds.), *Methods in Paleomagnetism* (pp. 254–286). Amsterdam: Elsevier.